Journal of ELECTRONIC MATERIALS, Vol. 46, No. 10, 2017
DOI: 10.1007/s11664-017-5620-8

Understanding Ferromagnetic Phase Stability, Electronic and Transport Properties of $BaPaO_3$ and $BaNpO_3$ from *Ab-Initio* Calculations

SHAKEEL AHMAD KHANDY[1,2] and DINESH C. GUPTA[1,3]

1.—Condensed Matter Theory Group, School of Studies in Physics, Jiwaji University, Gwalior, MP 474 011, India. 2.—e-mail: shakeelkhandy11@gmail.com. 3.—e-mail: sosfizix@gmail.com

An extensive study of rare-earth perovskite $BaPaO_3$ and $BaNpO_3$ has been performed by first-principles tactics based on density functional theory (DFT), because the delocalized *f*-electrons play an important role in the band structure formation, to reveal their impact on the overall physical and chemical properties; it has turned out to be an interesting theme. Along with critical radii and thermoelectric properties, two different theories are employed to calculate the structural properties. The DFT and empirically calculated lattice constants are in rational accord with the experimental results. The critical radius calculations show that the $BaPaO_3$ lattice has a smaller oxygen migration activation energy than the $BaNpO_3$. In addition, we discuss the band profile and magnetic moments for these materials, which demonstrate the half-metallic ferromagnetism with a direct energy gap of 3.91 eV for $BaPaO_3$ and an indirect gap of 3.79 eV for $BaNpO_3$. More interestingly, the integral magnetic moments are in accordance with the Slater–Pauling rule.

Key words: Perovskites, ferromagnetism, electronic structure, seebeck coefficient and electrical conductivity

INTRODUCTION

Worldwide attention in transition metal perovskite oxides over the past few decades can be credited to their important physical properties, including superconductivity, ferroelectricity, half-metallic ferromagnetism (HMF), metal–insulator transitions, colossal magnetoresistance, thermoelectricity, etc.[1-4] The exhibition of these functional properties within the transition metal perovskite oxides is undoubtly manifested due to the multifaceted and delicate interchange between the lattice, charge, orbital, and spin degrees of freedom. Reliable theoretical modeling and simulation plays a key role in the prediction of multidimensional properties of functional materials and to have in-depth investigation of the origins of interactions in these structures. The possibility of tailoring the structural, magneto-electronic and transport properties of a material with an applied field has received much interest from material scientists as well as industry for the reuse of waste energy and lower consumption in thermoelectric, spintronic and optoelectronic devices.[5-8] In view of the above, perovskites prove to be potential candidates for applications in such novel devices, therefore attracting huge demand from industry and technology.

Rare-earth (RE)-based cubic perovskites, including $BaPrO_3$, $BaCeO_3$, $BaThO_3$ and $BaUO_3$, have been investigated for their electronic, structural and magnetic properties.[9,10] $BaThO_3$, a significant fission reactor product, has been studied for its structural, thermodynamic and optoelectronic properties.[11-13] Since the reported experimental results for $BaNpO_3$[14,15] and $BaPaO_3$[16] are limited just to the structure, the electronic, magnetic and transport properties are still undiscovered; therefore, the present oxide materials of the same family need further investigation. The significant *f*-electron

(Received December 20, 2016; accepted May 22, 2017; published online June 9, 2017)

density in RE perovskite systems, even at larger distances rather than half-interatomic distances, interplays with the chemical bonds, magnetic phenomenon and crystal structure. Thus, probing their electronic band profile via magnetic and lattice structure studies turns out to be a stimulating task. We here investigate the structural, electronic, magnetic and transport properties of these compounds.

METHODOLOGY

All computations were performed using a full-potential linearized augmented plane wave method within the framework of density functional theory (DFT). For the exchange–correlation functional, we have employed the generalized gradient approximation GGA,[17] GGA + U[18] modified Becke Johnson mBJ[19] and spin–orbit coupling GGA + SOC.[20] Further, the muffin-tin radii have been selected on the assumption that the unit cell is divided into two regions, inside and outside the muffin-tin sphere. The spherical harmonic expansion and the plane wave basis set were chosen within and outside the muffin-tin sphere, respectively. The valence part is treated within a potential expanded into spherical harmonics up to l = 4. Within the atomic spheres, the maximum l quantum number for the wave expansion is confined to l_{max} = 10. The controlled size of the basis set via the convergence parameter $R_{MT}K_{max}$ set to 8.0 is chosen for the present calculations. The cut-off energy, i.e. the separation between the core and valence states is set to −7 Ry. For self-consistent calculations, we use 5000 k-points in the whole Brillouin zone (BZ) which corresponds to 150 k-points in the irreducible wedge of the BZ. The convergence criterion for the current study is considered when the total energy is stable within 0.001 Ry and the charge difference less than 0.001 e/a.u.^{3} per unit cell.

STRUCTURAL OPTIMIZATION

The present materials exhibit the perovskite-type structure with a chemical formula ABO_3, where the oxygen atoms form a regular octahedron surrounding the B atom. This type of structure belongs to the space group Pm − 3m (221). There is a single molecule in the elementary cell with Wychoff positions of atoms as Ba 1a (0, 0, 0), Pa/Np1b (0.5, 0.5, 0.5) and O 3c (0.5, 0.5, 0). In order to determine the most stable ground state structure of $BaREO_3$, we adopted the double cell volume optimization method in which 1 × 2 × 1 supercells for non-magnetic (NM), ferromagnetic (FM) and antiferromagnetic (AFM) phases are considered. In AFM phase, the spin of Pa/Np atoms is set as up (↑) in one cell and down (↓) in the second cell, while as it is kept up or down simultaneously for both the cells in the FM phase.[20] The energy optimization curves (Fig. 1a and b) for both the compounds clearly indicate that the FM state is energetically stable rather than the corresponding antiferromagnetic (AFM) and non-magnetic (NM) phases because of their minimized cohesive energy values in the FM phase. The optimized values of lattice constants, bulk moduli, derivatives of bulk modulus and total energies are reported in Table I, as procured from calculations of the structure optimization. Also, the data are compared with the measured records[14-16] as well as the empirical lattice constants calculated via the ionic radii method reported earlier.[20] The lattice constants decisively agree with the reported experimental results.

Bond lengths play a key role in defining the reliability of the perovskite structure. The calculated average bond lengths between different atoms in these compounds presented in Table I are used to calculate the tolerance factor (t) of a perovskite, and thereafter the crystal structure of the compound is predicted.[20]

$$t = 0.707\frac{<Ba-O>}{<RE-O>} \quad (1)$$

The DFT calculated bond lengths between RE (Pa and Np) and O decreases as we go from Pa to Np. This decrease is due to the larger size of Pa than Np, which in turn is instigated by lanthanide contraction. Also, the bond lengths between Ba-Pa/Np and Ba-O depict a similar trend. Generally, the tolerance factor (t) is a well-accepted empirical parameter to assign the stable structure for any perovskite compound. Materials with t = 0.9–1.0 have an ideal cubic structure, while t in the range 0.71–0.9 results in an orthorhombic or rhombohedral structure. Hexagonal or tetragonal structures have ($t > 1$) and if ($t < 0.71$) and the different structures are formed.[21-23] It is obvious from Table I that the calculated tolerance factor for $BaPaO_3$ is 0.99 and for $BaNpO_3$ is 1.00, which therefore confirm the stability of the cubic phase. The tolerance factors calculated by the ionic radii method[20] also confirm the cubic structure of these compounds.

The critical radius (r_C) for a perovskite is the narrowest passage through which the oxygen ion can migrate along the crystal. It plays an important role in the activation energy of oxygen migration and therefore the ionic conductivity. It describes the maximum size of the mobile ion that can pass through. It also offers a guideline for the selection of a dopant ion to tailor the desirable properties. The critical radii for both the compounds are calculated by using the following formula[24]:

$$r_C = \frac{a_0\left(\frac{3}{4}a_0 - \sqrt{2}r_{RE}\right)r_{RE} + r_{RE}^2 - r_{Ba}^2}{(2r_{Ba} - r_{RE}) + \sqrt{2}a_0} \quad (2)$$

where a_0 is the lattice constant, and r_{Ba} and r_{RE} are the ionic radii of Ba and Pa/Np atoms, respectively.

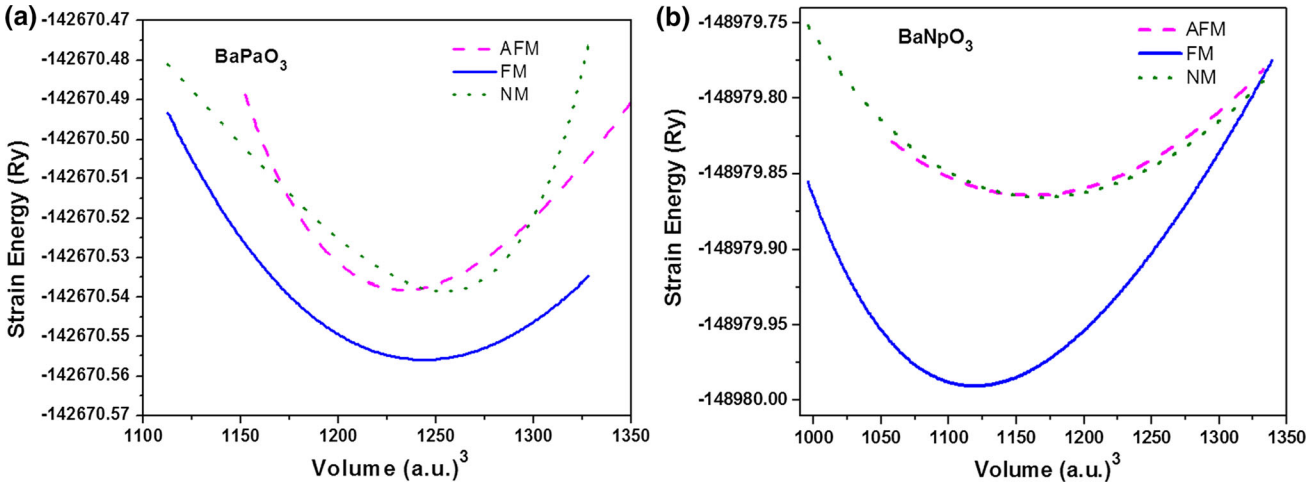

Fig. 1. Calculated double cell optimization curves for paramagnetic, ferromagnetic and anti-ferromagnetic phases of (**a**) $BaPaO_3$ and (**b**) $BaPaO_3$ in Pm − 3m configuration.

Table I. Calculated values of the lattice constant, unit cell volume, bulk modulus, derivative of bulk modulus, ground-state energy, critical radius and tolerance factor (*t*) of $BaREO_3$ compounds

Parameter	Present	Empirical	Expt.
$BaPaO_3$			
Lattice constant (Å)	4.51	4.43	4.45[16]
Volume (a.u)^3	62.71		
Bulk modulus (GPa)	114.8		
B' (GPa)	2.35		
Critical radius (r_C)	0.96		
Tolerance factor (t)	0.99	0.96	
Bond lengths (Å)			
Ba-O	3.19		
Ba-Pa	3.90		
Pa-O	2.25		
ΔE(Ry) = $E_{FM} - E_{AFM}$	−0.178		
$BaNpO_3$			
Lattice constant (Å)	4.43	4.38	4.38[14]
Volume (a.u)^3	590.04		
Bulk modulus (GPa)	120.85		
B' (GPa)	4.11		
Critical radius (r_C)	0.93		
Tolerance factor (t)	1.00	0.94	
Bond lengths (Å)			
Np-O	3.10		
Ba-NP	3.79		
Np-O	2.19		
ΔE(Ry) = $E_{FM} - E_{AFM}$	−0.126		

The greater the value of the critical radius, the smaller the migration activation energy, so that minimum lattice disturbance occurs. From the calculated values of the critical radii of both compounds, we can say that the oxygen ions can migrate more readily in the $BaPaO_3$ lattice, which generally leads to the enhancement in ionic conductivity.[24]

The nature of chemical bonding in materials is well explained by electronic charge density plots, since the formation of a chemical bond occurs when one or more electrons attract the two nuclei simultaneously. Figure 2 displays the charge density plots of $BaREO_3$ (RE = Pa and Np) in the (110) plane for both spin states. From the electron density distribution, the sharing of electrons between the RE atom (Pa or Np) and O is seen, which thus uncovers the covalent nature of the bond between them, whereas between Ba and RE, the ionic bond is present and in the spin-down case, the shifting of the shape of RE ions from almost spherical to dumbbell occurs, which shows ionic interactions of

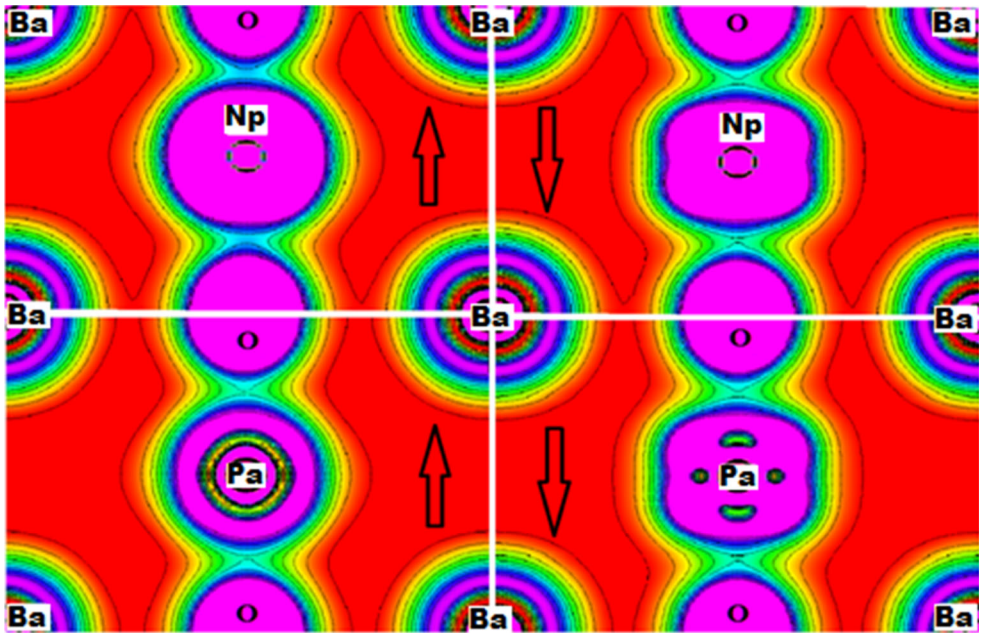

Fig. 2. Spin-dependent electronic charge densities in (110) plane of $BaREO_3$ (RE = Pa and Np).

rare-earth transition metal atoms with O and a stronger covalent bond between RE and O than in the spin-down case.

ELECTRONIC PROPERTIES

To have an overall picture of the electronic structure, the spin-polarized energy bands along the high symmetry directions of the Brillouin zone (BZ) have been studied for the cubic perovskites $BaPaO_3$ and $BaNpO_3$, as shown in Fig. 3. Almost similar band profiles with little difference are found for both the compounds by GGA. The half-metallic character is exhibited along with a direct band of 3.91 eV for $BaPaO_3$ along the Γ symmetry point, while there is an indirect band gap of 3.79 eV for $BaNpO_3$ existing at $R - \Gamma$ symmetry points in the spin-down states of both the materials. The valance band crosses the Fermi level and therefore presents the metallic nature in the spin-up state for these materials. The electronic polarization is responsible for the difference in the band gap energies in the high- and low-spin states. In Fig. 4, we have plotted the total and partial densities of states (DOS) for $BaREO_3$ to explain the contribution of different states in the band structures. As seen from the partial DOS, strong overlapping of Pa/Np-*f* (pink color) and Ba-d (maroon color) states is found around the Fermi level with a little contribution from the Pa-d bands. Unlike the traditional *p–d* hybridization which is frequently found in perovskites, *d–f* hybridization between Ba and RE atoms takes place. However, the *p*-states of the Ba and O atoms are present in the valence band and the Ba-f states in the conduction band, as shown by color-filled regions in Fig. 3, are very far from the Fermi level for both compounds. A noticeable role in the overall physical properties is mainly established by the RE-*5f*, Ba-*5d* and RE-*6d* states in these perovskites. The localization of the *f*-bands at the Fermi level makes these compounds metallic in the spin-up phase and semiconducting in the spin-down state. Further, the application of onsite coulomb interaction (GGA + U) and mBJ as well as GGA + SOC was carried out to fully understand the role of intricate *f*-electrons in the energy gap and therefore the band formation. The U_{eff} $(U - J)$ variation was performed over a wide range of 0.1–8.0 eV and the U_{eff} up to such a maximum does not make the RE-*f* electrons delocalized, i.e. a peak of 10 eV still appears at the Fermi level in the spin-up state as seen from the DOS, and thereby felicitating a small effect on the metallic nature of both these materials in the spin-up state. This peak at the Fermi level is due to the *5f*-electrons of Pa/Np as seen from the partial DOS plotted in Fig. 3. In the spin-down state, only the top of the valence band shifts towards the Fermi level and the conduction band accordingly shifts away from it, rendering an almost feeble increase in the energy gaps. Thus, the half-metallic nature is retained even at U_{eff} = 8 eV. Similarly, the mBJ and GGA + SOC calculations display the analogous results with a small difference, as seen in Fig. 5. On applying the above exchange–correlation potentials, the *f*-bands still appear at the Fermi level in the spin-up phase in both oxides. Henceforth, it is well established that these materials are half-metallic in nature.

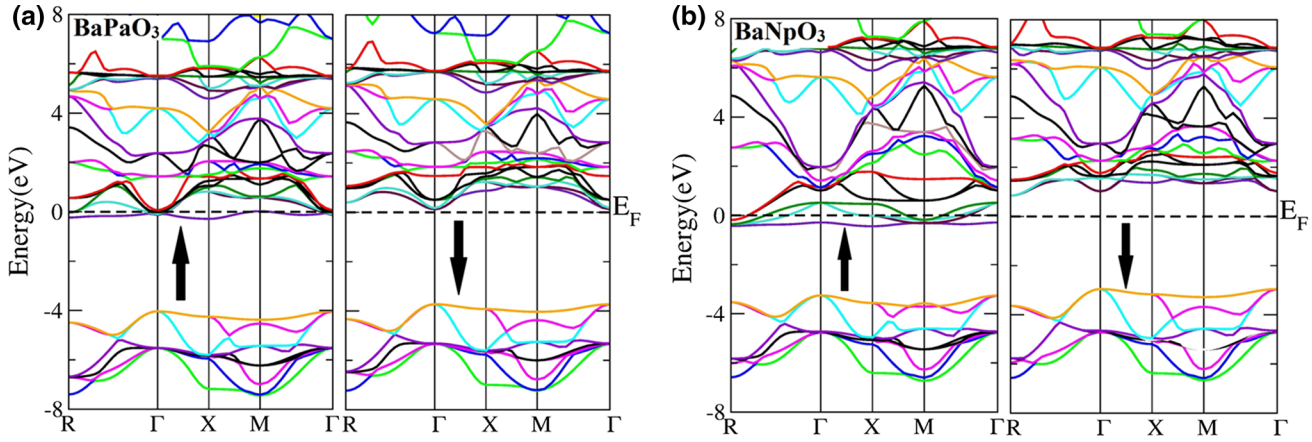

Fig. 3. Spin-resolved band structures (**a**) $BaPaO_3$ and (**b**) $BaPaO_3$ at equilibrium lattice constant calculated by GGA approach.

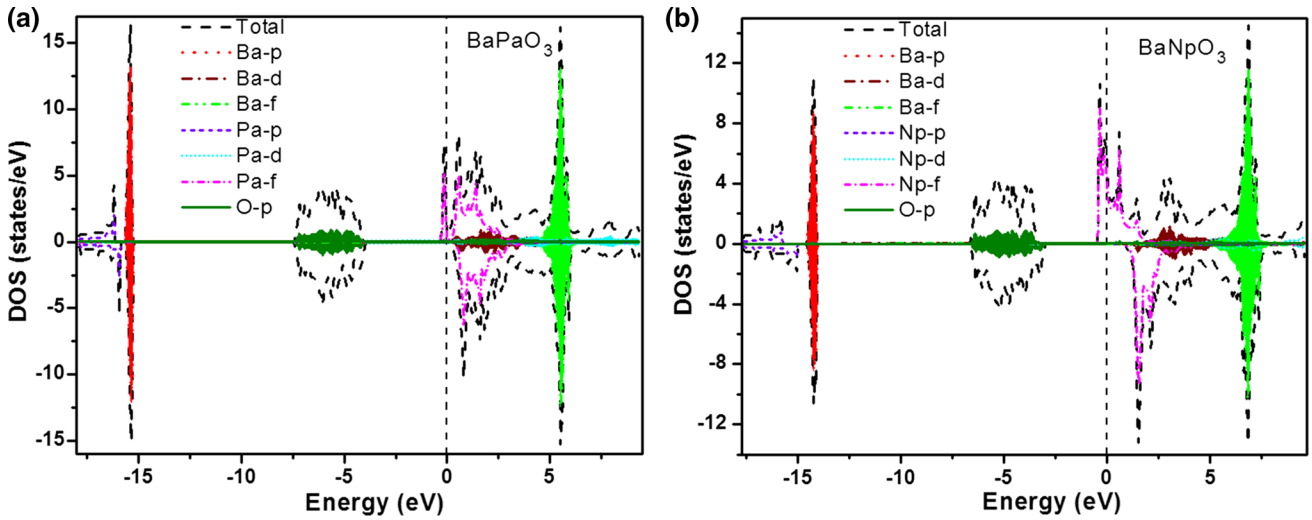

Fig. 4. Spin-polarized partial densities of states (pDOS) for (**a**) $BaPaO_3$ and (**b**) $BaPaO_3$ at equilibrium lattice constant calculated by GGA approach.

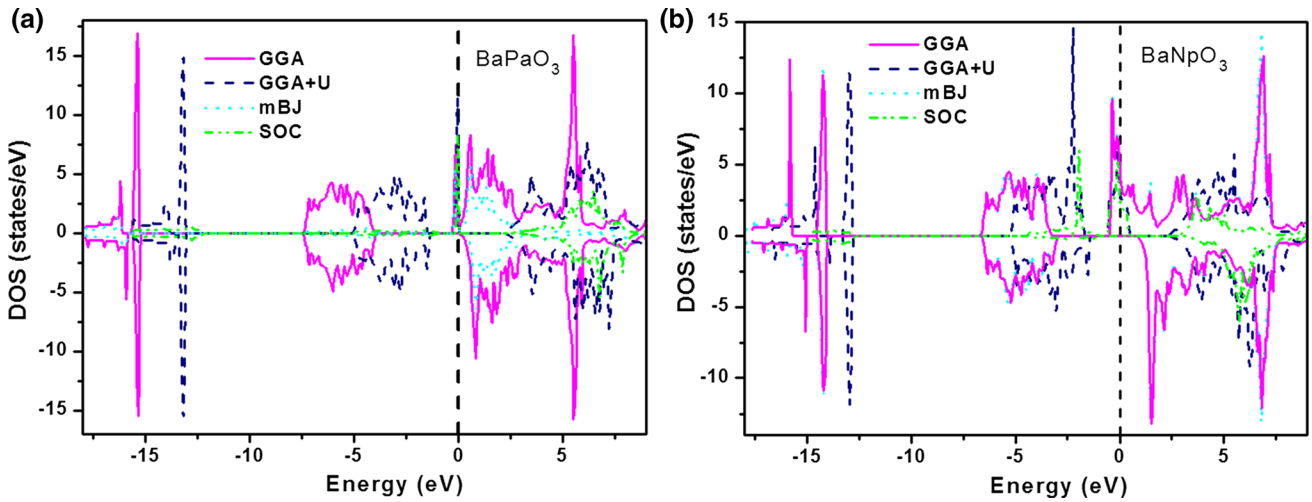

Fig. 5. Spin-polarized total densities of states (DOS) for (**a**) $BaPaO_3$ and (**b**) $BaNpO_3$ calculated by GGA, GGA + U, mBJ and GGA + SOC methods.

MAGNETIC PROPERTIES

The magnetic phase stability for these compounds has been perceived by double-cell optimization (Fig. 1). The total, interstitial and individual magnetic moments for both the materials are listed in Table II. For GGA calculations, the total magnetic moments for $BaPaO_3$ and $BaNpO_3$ are 1.0 μB and 3.0 μB, respectively, while for GGA + U and mBJ, the corresponding values are almost the same. The magnetic moment of O being small, but negative, is due to the occurrence of anti-ferromagnetic coupling between O-Ba and O-Pa/Np atoms. Thus, it has been established in the present study that the Np-atom shows more ferromagnetic response than the Pa-atom with ferromagnetic interaction. The observed integral value of total magnetic moment is generally a property of half-metallic Heusler alloys. Remarkably, they follow the Slater–Pauling rule ($Z_t - 24$), where Z_t is the total number of valence electrons in the constituent atoms of the crystal.[25,26] Therefore, our results along with semiconducting energy gaps may potentially motivate these members of the perovskite family as spintronic materials.

Also, magnetic susceptibility from post-DFT[27] treatment was calculated to recognize the magnetic ground state. By analyzing the susceptibility plots shown in Fig. 6, the reciprocal of the susceptibility curve clearly depicts the positive value of the Curie–Wiess constant (T_θ) $\sim$ 45 K and $\sim$50 K for $BaPaO_3$ and $BaNpO_3$, respectively. Since, $T_\theta > 0$, ferromagnetic interactions, which therefore explains that the Curie–Wiess law[20] is obeyed, and the ferromagnetic phase is the stable ground state for both the compounds.

TRANSPORT PROPERTIES

Post-DFT treatment along with independent time approximation within the framework of Boltzman theory has been employed in the present work to elucidate the transport properties of $BaREO_3$ compounds. The transport coefficients σ, k, and S as a function of temperature (T) and chemical potential (μ) are obtained from the following equations.

$$\sigma = \frac{1}{\Omega}\int \Xi_{i,k}\left[\frac{\partial f_0(T,\varepsilon)}{\partial \varepsilon}\right]d\varepsilon \tag{3}$$

$$k = \frac{1}{e^2\Omega}k_B^2 T\int \Xi_{i,k}\left(\frac{\varepsilon-\mu}{k_B T}\right)^2\left[-\frac{\partial f_0(T,\varepsilon)}{\partial \varepsilon}\right]d\varepsilon \tag{4}$$

where Ω is the volume of the unit cell and f_0 is the Fermi–Dirac distribution function and $\Xi_{i,k}$ is the transport distribution kernel defined elsewhere.[28-30] And, lastly, the total Seebeck coefficient is evaluated by the two-current model[31] using Eq. 5 to reproduce the thermoelectric figure-of-merit (zT) for these oxide materials.

$$S = \frac{\sigma(\uparrow)S(\uparrow) + \sigma(\downarrow)S(\downarrow)}{\sigma(\uparrow) + \sigma(\downarrow)} \tag{5}$$

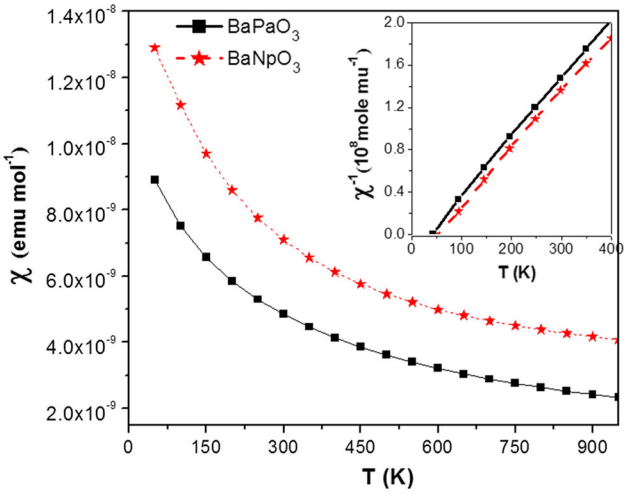

Fig. 6. Magnetic susceptibility (χ) and its inverse (χ^{-1}) as a function of temperature for $BaPaO_3$ and $BaNpO_3$ compounds.

Table II. Calculated values of total, individual, interstitial spin moments in Bohr magneton (μB) and band gap (in eV) of $BaPaO_3$ and $BaNpO_3$ by GGA, GGA + U, mBJ and GGA + SOC methods

Compound	μ_{Ba}	$\mu_{Pa/Np}$	μ_O	$\mu_{Int.}$	μ_{Total}	Band gap
$BaPaO_3$						
GGA	0.03	0.07	−0.02	0.25	1.00	3.91
GGA + U	0.01	0.87	−0.02	0.18	1.05	3.89
mBJ	0.04	0.75	−0.02	0.28	1.05	4.00
SOC	0.02	0.80	−0.02	0.24	1.06	3.95
$BaNpO_3$						
GGA	0.02	2.60	−0.07	0.45	3.00	3.79
GGA + U	0.02	2.67	−0.07	0.40	3.02	3.75
mBJ	0.02	2.76	−0.08	0.41	3.11	3.84
SOC	0.02	2.71	−0.07	0.42	3.22	3.81

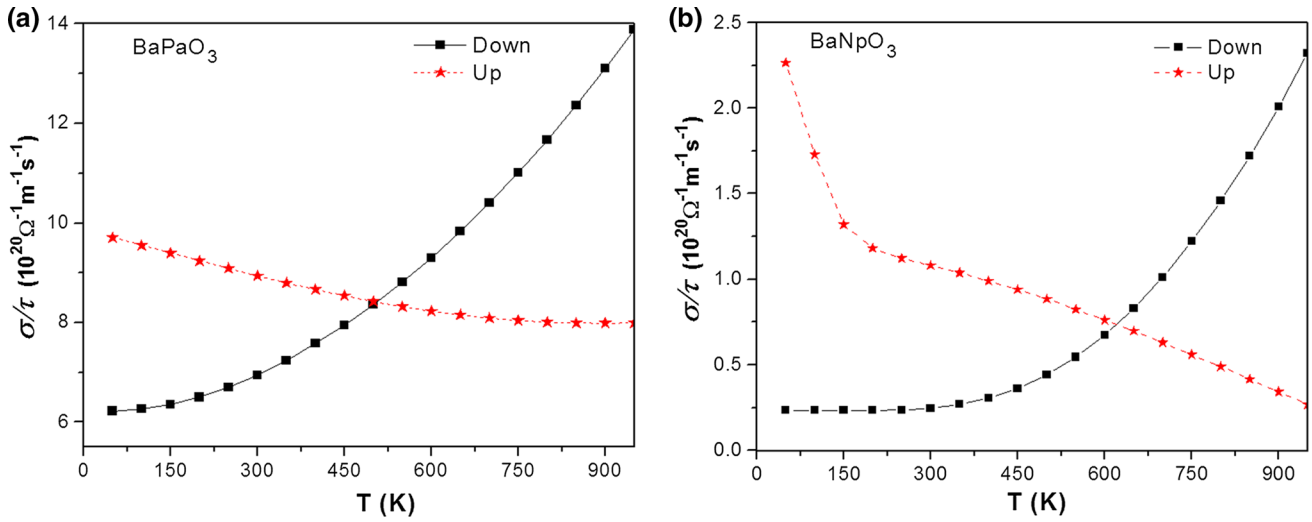

Fig. 7. Electrical conductivity versus temperature plots for (**a**) $BaPaO_3$ and (**b**) $BaNpO_3$ in both the spin states. (τ) is the relaxation time.

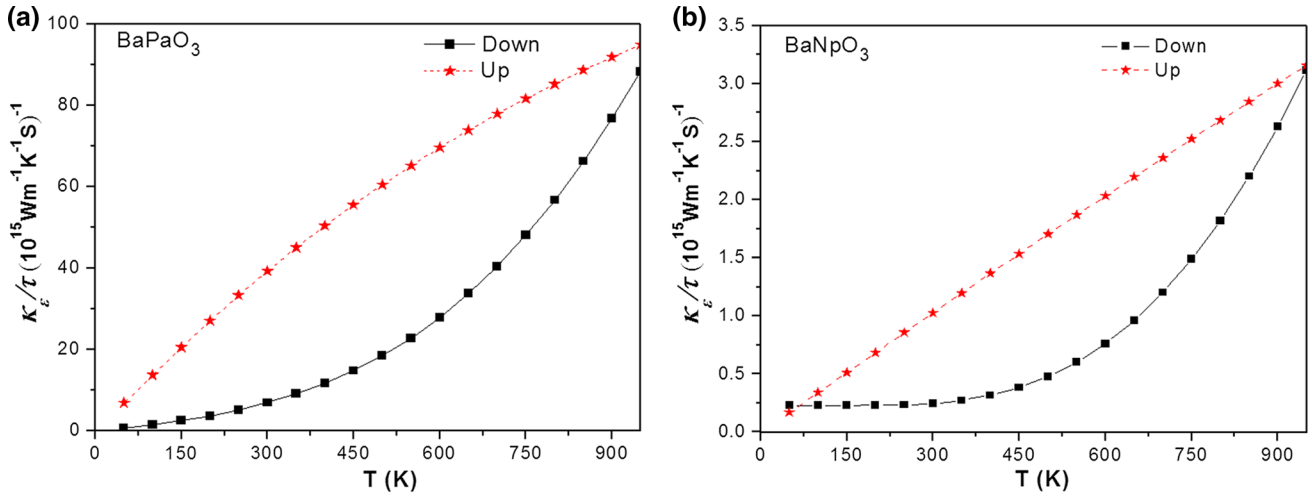

Fig. 8. Electronic thermal conductivity (κ_e/τ) as a function of temperature for (**a**) $BaPaO_3$ and (**b**) $BaNpO_3$ perovskites.

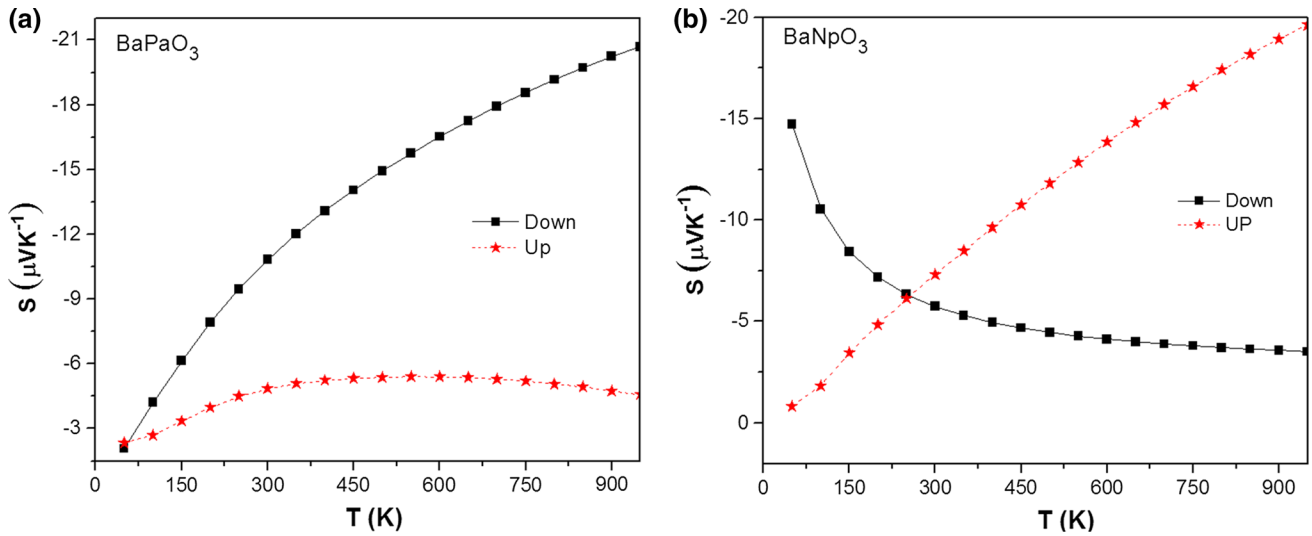

Fig. 9. Calculated Seebeck coefficient (S) of (**a**) $BaPaO_3$ and (**b**) $BaNpO_3$ in both spin-up and spin-down channels.

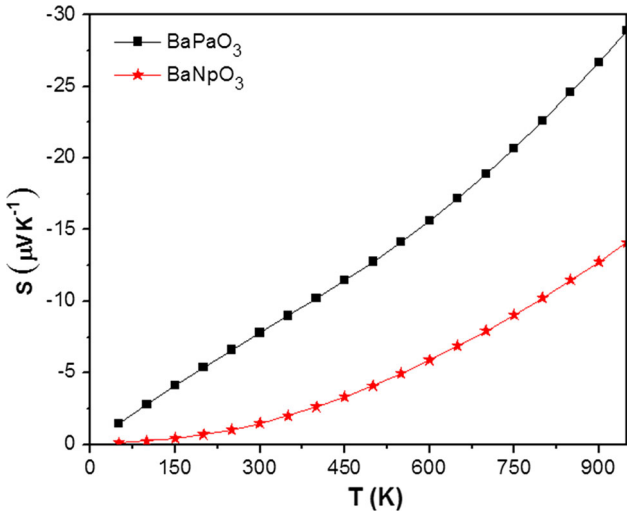

Fig. 10. Total Seebeck coefficient (S) of $BaREO_3$ compounds calculated by the two-current model.

The temperature variation of electrical conductivity (σ/τ) as depicted in Fig. 7 describes almost a linear increase for the spin-down state, from $\sim 9.8 \times 10^{20} (\Omega ms)^{-1}$ at 50 K to $8.3 \times 10^{20} (\Omega ms)^{-1}$ at 800 K of $BaPaO_3$ and $\sim 22.7 \times 10^{20} (\Omega ms)^{-1}$ at 50 K to $2.5 \times 10^{20} (\Omega ms)^{-1}$ at 950 K of $BaPaO_3$, therefore confirming the semiconducting nature in the spin-down channel. But, a decreasing trend observed in spin-up state concludes the metallicity for both the materials.[32] Since κ comprises the electronic part, ε, and lattice, λ, contributions of thermal conductivity, the BoltzTrap is not able to calculate the latter part which is due to the phonon contributions of a lattice and therefore the thermal conductivity is underestimated. Hence, the observed κ_ε/τ versus T in Fig. 8 is perceived to be linear for both the oxides in the spin-up as well as the spin-down state.

The individual Seebeck coefficient (S) as a function of temperature plotted in Fig. 9 is negative for both materials in the entire temperature range for the spin-up as well as spin-down phase, which proposes the electrons as charge carriers, while the positive value of S suggests the holes as charge carriers. The variation of S with temperature for $BaPaO_3$ in both the spin channels shows an increasing trend, but,for $BaNpO_3$, a sharp decrease at lower temperatures in the S value of the spin-down channel is explained by the depopulation of the phonon modes.[33] The calculated total S values at room temperature presented in Fig. 10 are ~ 91 μV/K and ~ 20 μV/K for $BaPaO_3$ and $BaNpO_3$, respectively. Thereafter, the temperature-dependent zT has been estimated from the measured data of electrical, thermal and Seebeck coefficients. The observed values of zT at 300 K for $BaPaO_3$ and $BaNpO_3$ are 0.34 and 0.26, respectively. Due to the lack of any experimental or theoretical data, our calculations are therefore predictive results achieved for the present materials, which can offer valuable information and reference data for future researchers and the scientific community.

CONCLUSION

In summary, we have utilized the all-electron spin-polarized DFT-GGA, GGA + U and mBJ methods in this study to self-consistently predict structural, magneto-electronic and transport properties of cubic perovskites ($BaREO_3$). The structural parameters and geometries of the material are elucidated by DFT as well as by ionic radii methods and are found to be in close agreement with experiments. The nature of bonding between the different atoms is elaborated by the electron densities in the (100) plane. The relative stability of these compounds is discussed using total energies. The electronic band structures along with overall DOS and calculated magnetic moments reveal the half-metallic and ferromagnetic nature of these perovskites.

ACKNOWLEDGEMENT

The authors acknowledge the UGC (New Delhi) and Jiwaji University Gwalior (M.P) INDIA for financial support.

REFERENCES

1. N.C. Bristowe, J. Varignon, D. Fontaine, E. Bousquet, and P. Ghosez, *Nat. Commun.* 6, 6677 (2015).
2. P. Zubko, S. Gariglio, M. Gabay, P. Ghosez, and J.M. Triscone, *Annu. Rev. Condens. Matter Phys.* 2, 141 (2011).
3. M. Imada, A. Fujimori, and Y. Tokura, *Mod. Phys.* 70, 1039 (1998).
4. Y. Tokura and N. Nagaosa, *Science* 288, 462 (2000).
5. E. Dagotto, *Science* 309, 257 (2005).
6. M. Bibes and A. Barthélémy, *Nat. Mater.* 7, 425 (2008).
7. J. Scott, *Nat. Mater.* 6, 256 (2007).
8. H.Y. Hwang, Y. Iwasa, M. Kawasaki, B. Keimer, N. Nagaosa, and Y. Tokura, *Nat. Mater.* 11, 103 (2012).
9. K.A. Furøy, R. Haugsrud, M. Hänsel, A. Magrasó, and T. Norby, *Solid State Ion.* 178, 461 (2007).
10. Y. Hinatsu, *J Alloys Compd.* 193, 113 (1993).
11. A. Mitsui, M. Miyayama, and H. Yanagida, *Solid State Ion.* 22, 213 (1987).
12. A.V. Soldatov, D. Lamoen, M.J. Konstantinovic, S. Van den Berghe, A.C. Scheinost, and M. Verwerft, *J. Solid State Chem.* 180, 54 (2007).
13. R.L. Moreira and A. Dias, *J. Phys. Chem. Solids* 68, 1617 (2007).
14. B. Kanellakopulos, C. Keller, R. Klenze, and H. Stollenwerk, *Phys. B* 102, 221 (1980).
15. E. König, C. Rudowicz, V.P. Desai, and B. Kanellakopulos, *J. Chem. Phys.* 78, 5764 (1983).
16. H.J. Emeléus and A.G. Sharpe, *Advances in Inorganic Chemistry and Radiochemistry*, Vol. 12 (New York: Academic Press, 1969).
17. P. Blaha, K. Schwarz, and Comp Luitz, *Phys. Commun.* 59, 399 (1990).
18. S.L. Dudarev, G.A. Botton, S.Y. Savrasov, C.J. Humphreys, and A.P. Sutton, *Phys. Rev. B* 57, 1505 (1998).
19. F. Tran and P. Blaha, *Phys. Rev. Lett.* 102, 226401 (2009).
20. S.A. Khandy and D.C. Gupta, *RSC. Adv.* 65, 48009 (2016).
21. L.E. Russel, D.L. Harrison, and N.H. Brett, *J. Nucl. Mater.* 2, 310 (1960).
22. Z. Li, M. Yang, J.S. Park, S.H. Wei, J.J. Berry, and K. Zhu, *Chem. Mater.* 28, 284 (2016).

23. W. Travis, E.N.K. Glover, H. Bronstein, D.O. Scanlon, and R.G. Palgrave, *Chem. Sci.* 7, 4548 (2016).
24. J. Richter, P. Holtappels, T. Graule, T. Nakamura, and L.J. Gauckler, *Monatsh. Chem.* 140, 985 (2009).
25. T.M. Bhat and D.C. Gupta, *RSC Adv.* 6, 80302 (2016).
26. S. Yousuf and D.C. Gupta, *Mater. Chem. Phys.* 192, 33 (2017).
27. G.K.H. Madsen and D.J. Singh, *Comput. Phys. Commun.* 175, 67 (2006).
28. T.M. Bhat and D.C. Gupta, *J. Electron. Mater.* 45, 6012 (2016).
29. G.D. Mahan and J.O. Sofo, The best thermoelectric. *Proc. Natl. Acad. Sci. USA* 9, 7436 (1996).
30. S.A. Khandy and D.C. Gupta, *RSC Adv.* 6, 97641 (2016).
31. T.M. Bhat and D.C. Gupta, *J. Magn. Magn. Mater.* 435, 173 (2017).
32. S. Yousuf and D.C. Gupta, *Mater. Sci. Eng. B* 221, 73 (2017).
33. J.P.A. Makongo, D.K. Misra, X.Y. Zhou, A. Pant, M.R. Shabetai, X.L. Su, C. Uher, K.L. Stokes, and P.F.P. Poudeu, *J. Am. Chem. Soc.* 133, 18843 (2011).